



## Higher Efficiency Perovskite Solar Cells Using Au@SiO<sub>2</sub> Core-Shell Nanoparticles

Journal:	<i>Sustainable Energy &amp; Fuels</i>
Manuscript ID	SE-ART-09-2017-000472.R2
Article Type:	Paper
Date Submitted by the Author:	24-Jun-2018
Complete List of Authors:	<p>Chandrasekhar, Pakanati; IIT Delhi, Centre for Energy Studies            Dubey, Ashish; SDSU, Electrical Engineering            Reza, Khan; SDSU, Electrical Engineering            Hasan, MD Nazmul; South Dakota State University, Electrical Engineering &amp; Computer Science            Bahrami, Behzad; South Dakota State University,            Komarala, Vamsi; Indian Institute of Technology, Centre for Energy Studies            Hoefelmeyer, James; The University of South Dakota, Chemistry            He, Qingquan; South Dakota State University            Wu, Fan; Huzhou University, School of Science and Key Lab of Optoelectronic Materials and Devices            Qiao, Hui; South Dakota State University            Zhang, Wen-Hua; Institute of Chemical Materials, China Academy of Engineering Physics, ; Dalian Institute of Chemical Physics, Chinese Academy of Sciences,            Qiao, Qiquan; South Dakota State University, Center for Advanced Photovoltaics</p>

## Higher Efficiency Perovskite Solar Cells Using Au@SiO<sub>2</sub> Core-Shell Nanoparticles

P. S. Chandrasekhar<sup>1,2</sup>, Ashish Dubey<sup>1</sup>, Khan Mamun Reza<sup>1</sup>, MD Nazmul Hasan<sup>1</sup>, Behzad Bahrami<sup>1</sup>, Vamsi K. Komarala<sup>2</sup>, James D. Hoefelmeyer<sup>4</sup>, Qingquan He<sup>1</sup>, Fan Wu<sup>1</sup>, Hui Qiao<sup>1</sup>, Wen-Hua Zhang<sup>3\*</sup> and Qiquan Qiao<sup>1\*</sup>

<sup>1</sup>Center for Advanced Photovoltaics, Department of Electrical Engineering and Computer Science, South Dakota State University, Brookings, SD 57007, USA

Tel: 1-605-688-6965; Fax: 1-605-688-4401;

\*Email: [Qiquan.Qiao@sdstate.edu](mailto:Qiquan.Qiao@sdstate.edu)

<sup>2</sup>Center for Energy Studies, Indian Institute of Technology Delhi, New Delhi-110016, INDIA

Tel; +91 11 2659 1255; Fax: +91 11 2659 1251

<sup>3</sup>Sichuan Research Center of New Materials, Institute of Chemical Materials, China Academy of Engineering Physics, Chengdu, P. R. China

\*Email: [whzhang@caep.cn](mailto:whzhang@caep.cn)

<sup>4</sup>Department of Chemistry, University of South Dakota, 414 E. Clark St., Vermillion, SD 57069

**Abstract:** In this work, we improved photovoltaic performance by about 27% in planar p-i-n perovskite solar cells (PSCs) using plasmonic Au@SiO<sub>2</sub> core-shell nanoparticles (NPs). The devices have an architecture of ITO glass/PEDOT: PSS/perovskite(CH<sub>3</sub>NH<sub>3</sub>PbI<sub>3</sub>)/PCBM/Rhodamine/Ag. Four batches of devices were fabricated with different concentrations of Au@SiO<sub>2</sub> NPs ranging from 0.4 to 1.6 wt.% with an interval of 0.4wt%. The Au@SiO<sub>2</sub> NPs were integrated at the interface between PEDOT: PSS layer and the active perovskite layer. At an optimized concentration of 1.2 wt. % Au@SiO<sub>2</sub> NPs, the PSCs achieved a 25.1% of enhancement in photocurrent from 17.45 to 22.35 mA/cm<sup>2</sup> and an improvement of 27.3% in power conversion efficiency (PCE) from 11.44 to 14.57%. This significant improvement in device performance is attributed to the localized surface plasmon resonance (LSPR) of Au@SiO<sub>2</sub> NPs, which enhanced the light absorption in the active perovskite layer. The transient photocurrent and photovoltage measurements revealed that PSCs with Au@SiO<sub>2</sub> NPs have faster charge transport time and longer recombination lifetime than those without Au@SiO<sub>2</sub> NPs. These results demonstrate that plasmonic metal nanoparticles substantially improved the efficiency of PSCs.

**Keywords:** Perovskite solar cells, Au@SiO<sub>2</sub> nanoparticles, Surface plasmon resonances, Light absorption

## 1. Introduction

Organic-inorganic hybrid metal halide (CH<sub>3</sub>NH<sub>3</sub>PbX<sub>3</sub>, X = Cl, Br and I) perovskite solar cells (PSCs) have attained a great interest in photovoltaic community due to their tremendous improvement in power conversion efficiency (PCE). The enhancement in PCE is due to unique properties of hybrid perovskite materials such as high absorption coefficient, long charge carrier diffusion lengths, low cost and simple fabrication procedures make it widely studied solar cell technology<sup>1-5</sup>. In 2009, Miyasaka *et al.* first reported the perovskite (CH<sub>3</sub>NH<sub>3</sub>PbI<sub>3</sub>) solar cells with a PCE of 3.8%<sup>6</sup>. Currently, the PCE of PSCs was reported about 22% and they have shown a potential to reach the PCE of crystalline silicon (Si) solar cells<sup>7-9</sup>. In order to enhance the PCE and stability of PSCs, several strategies and fabrication techniques are employed for improving the crystallinity, electronic properties of perovskite thin film and charge transportation in the device<sup>8,10-14</sup>.

To further enhance the efficiency of PSCs, one of the finest approaches is to employ plasmonic metal nanoparticles (NPs) in between device layers for improving optical absorption in perovskite thin film without causing any changes in perovskite layer and the device structure. Under light illumination, metal NPs produce localized surface plasmon resonances (LSPRs). Thus the collective oscillations of surface electrons on metallic nanostructures with confined electromagnetic energy will improve light absorption of the active medium surrounding metal NPs<sup>15-17</sup>. This phenomenon has been well studied in polymer solar cells, DSSCs and in Si solar cells for achieving high photovoltaic performance<sup>18-22</sup>. Jang *et al.* clearly addressed the plasmonic enhancement mechanisms in all photovoltaic devices ranging from conventional Si

solar cells to DSSCs, organic and perovskite solar cells<sup>23</sup>. Snaith *et al.* demonstrated the enhancement in photocurrent and PCE in meso-superstructure PSCs by incorporating Au@SiO<sub>2</sub> NPs inside the Al<sub>2</sub>O<sub>3</sub> matrix. The origin of improvement in photocurrent and PCE was attributed to the reduced exciton binding energy rather than enhanced light absorption<sup>24</sup>. In another study, Snaith and co-workers reported a significant enhancement in photocurrent and PCE by incorporating Ag@TiO<sub>2</sub> NPs in the active layer of the device. They proposed a theoretical model in which highly polarizable metal NPs improve an optical path length by acting as antennas for increasing reabsorption of emitted radiation<sup>25</sup>. Sun and co-workers addressed a unique sandwich structure of TiO<sub>x</sub>/Au NPs/TiO<sub>x</sub> in PSCs and observed an improved charge carrier transportation by the assistance of plasmonic-mediated hot carrier injection at the metal-semiconductor Schottky junction<sup>26</sup>. Recently, Park *et al.* reported an improvement in photovoltaic performance of PSCs by embedding Au NPs into the Spiro-OMeTAD hole transport layer<sup>27</sup>.

Herein, we successfully incorporated different concentrations (0.4, 0.8, 1.2 and 1.6wt. %) of Au@SiO<sub>2</sub> core-shell NPs at the interface between the PEDOT: PSS hole transport layer and an active perovskite (CH<sub>3</sub>NH<sub>3</sub>PbI<sub>3</sub>) layer. At an optimized concentration (1.2wt. %) of Au@SiO<sub>2</sub> NPs, we obtained a significant improvement in photocurrent by 25.1% from 17.45 to 22.35 mA/cm<sup>2</sup> and PCE by 27.3% from 11.44 to 14.57%. The improved photovoltaic performance is attributed to an increased light absorption, enhanced charge transportation across the interface between perovskite layer and hole transport layer.

## 2. Experimental Section

### 2.1. Materials

Chloroauric acid ( $\text{HAuCl}_4 \cdot 3\text{H}_2\text{O}$ , >99%), Tetraethoxysilane (TEOS, >99%), Ammonia (30 wt.%  $\text{NH}_3$  in water) and lead iodide ( $\text{PbI}_2$ , 99%) were obtained from Acros Organics. Poly(vinylpyrrolidone) with an average molar mass of 40 Kg/mol (PVP – 40), anhydrous dimethyl sulphoxide (DMSO, 99.9%),  $\gamma$ -butyrolactone (99%), Rhodamine, ethanol (EtOH) and acetone were purchased from Sigma-Aldrich. Methylammonium iodide ( $\text{CH}_3\text{NH}_3\text{I}$ ) was purchased from DyeSol (Australia). PEDOT: PSS (Clevios<sup>TM</sup> PVP AI 4083) was obtained from Heraeus.  $\text{PC}_{60}\text{BM}$  was purchased from Nano-C. All materials were used as received without any modification.

## ***2.2. Device fabrication***

Indium-doped tin dioxide (ITO) coated glass substrates were cleaned sequentially with a detergent, deionized water, acetone and isopropyl alcohol for 30 min by an ultrasonication treatment and finally subjected to oxygen plasma treatment for 25 min. A PEDOT: PSS layer was deposited on cleaned ITO glass substrates by spin coating at a speed of 4500 rpm for 90 s, followed by annealing at 145 °C for 10 min. For the plasmonic PSCs, Au@SiO<sub>2</sub> core-shell NPs dispersed in ethanol with different concentrations were spun on top of PEDOT: PSS film with a spin speed of 3000 rpm for 30 s, followed by annealing at 125 °C for 5 min. The plasmonic Au@SiO<sub>2</sub> core-shell NPs were synthesized by a two-step method. Initially, Au NPs without SiO<sub>2</sub> shell were synthesized according to the standard sodium citrate reduction method, and followed by preparing a SiO<sub>2</sub> shell over Au NPs using tetraethyl orthosilicate (TEOS) by dispersing Au NPs in a solution of ammonia in ethanol<sup>28, 29</sup>. The Au@SiO<sub>2</sub> core-shell NPs deposited over PEDOT: PSS films were transferred to a nitrogen ( $\text{N}_2$ ) filled glove-box for depositing an active perovskite layer. The perovskite precursor solution was prepared by dissolving  $\text{CH}_3\text{NH}_3\text{I}$  (209 mg) and  $\text{PbI}_2$  (581 mg) in a mixed solvent of 3:7 volume ratio of DMSO and  $\gamma$ -butyrolactone,

which was kept at 70 °C with continuous stirring for overnight. The freshly prepared perovskite precursor solution was spin coated using two step method at a speed of 750 rpm for 20 s and 4500 rpm for 60 s. 160  $\mu$ l toluene was dropped in second step while spinning after 40 s, followed by annealing at 90 °C for 10 min. The Phenyl-C61-butyric acid methyl ester (PCBM, 20 mg/ml in chlorobenzene) was spin coated on perovskite films with a spin speed of 2000 rpm for 40 s and followed by annealing at 80 °C for 5 min. Rhodamine buffer layer (0.5 mg/ml in isopropyl alcohol) was spun with a speed of 4000 rpm for 40 sec. Finally, silver (Ag) electrode ( $\sim$ 80 nm) was evaporated under a high vacuum of  $2 \times 10^{-6}$  torr using a shadow mask with an active area of 0.16 cm<sup>2</sup>.

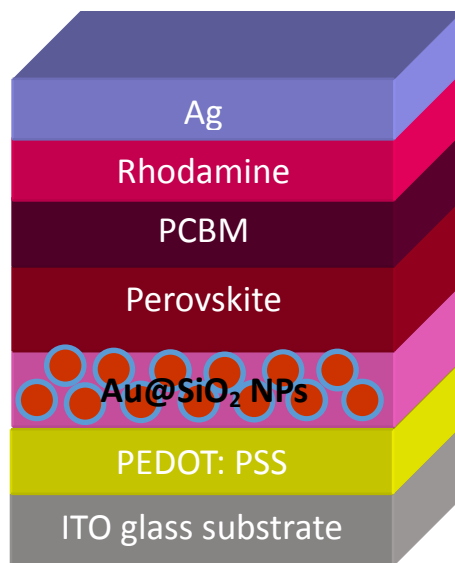
### **2.3. Characterization**

The morphology of as synthesized Au@SiO<sub>2</sub> core-shell NPs was analyzed using transmission electron microscopy (TEM, Technai G<sup>2</sup>). The absorption spectra of Au and Au@SiO<sub>2</sub> core-shell NPs and perovskite films with Au@SiO<sub>2</sub> core-shell NPs were characterized by UV-visible-NIR spectrophotometer (Agilent, G1103A). Scanning electron microscopy (SEM, Hitachi-S-4300N) and atomic force microscopy (AFM, Agilent 5500) were employed to analyze the surface morphology of perovskite films with and without Au@SiO<sub>2</sub> core-shell NPs. Current density-voltage (J-V) characteristics were measured by an Agilent 4155C semiconductor parameter analyzer under an illumination of one sun condition (AM 1.5G, 100 mW/cm<sup>2</sup>) equipped with a Xenon arc lamp (AM 1.5 filter, Newport). Prior to the measurements, a National Renewable Energy Laboratory (NREL) calibrated photodetector was used to calibrate the distance between device and Xenon arc lamp to ensure the light intensity of one sun condition. Incident photon to current conversion efficiency (IPCE) measurements were conducted by a Xenon arc lamp attached to a monochromator (Newport). Transient photocurrent and

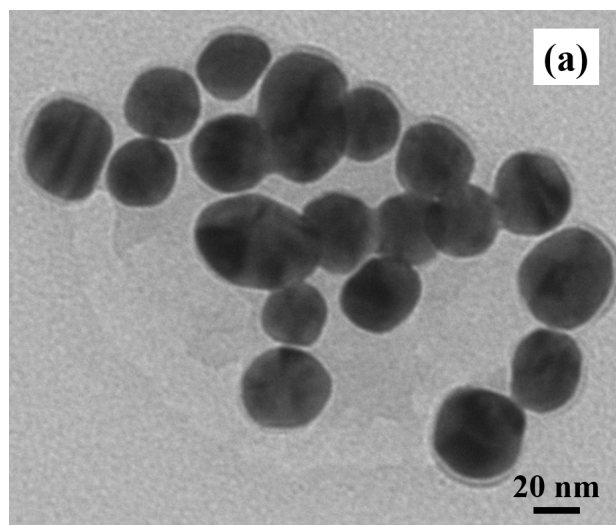
photovoltage measurements were carried out using a mixed signal oscilloscope (Agilent Technologies, MSO-X 4154A) attached with a nitrogen -dye laser.

### 3. Results and Discussion

The PSCs having a device architecture (ITO/PEDOT: PSS/CH<sub>3</sub>NH<sub>3</sub>PbI<sub>3</sub>/PCBM/Ag) is shown in Fig. 1. Au@SiO<sub>2</sub> core-shell NPs are introduced at an interface of PEDOT: PSS layer and perovskite layer. The morphology of as-synthesized Au@SiO<sub>2</sub> core-shell NPs are presented in Fig. 2a. It was observed that the Au core size is around 40 nm in diameter and coated with an approximate 2 nm of a thin SiO<sub>2</sub> shell. Without SiO<sub>2</sub> shell, the bare Au NPs will act as recombination centers when in contact with the perovskite material. Therefore, to protect the Au NPs, a thin SiO<sub>2</sub> shell was coated around the bare Au NPs. The absorption spectra of Au NPs with and without SiO<sub>2</sub> shell dispersed in ethanol are shown in Fig. 2b. The bare Au NPs showed a SPR peak at around 527 nm, and for the Au@SiO<sub>2</sub>, the SPR peak was observed at ~ 535 nm. The slight red shift in the absorption spectrum for Au@SiO<sub>2</sub> is attributed to a change in the local refractive index of the surrounding medium upon the addition of a thin SiO<sub>2</sub> shell<sup>30</sup>. It is very critical to protect the bare metallic NPs (Au/Ag) by coating with either titania (TiO<sub>2</sub>) or silica (SiO<sub>2</sub>) shell to minimize the charge carrier recombination in the photoactive layer for photovoltaic applications<sup>31,32</sup>.



**Figure 1.** Schematic of a PSC architecture by incorporating Au@SiO<sub>2</sub> NPs between PEDOT:PSS and perovskite layer.



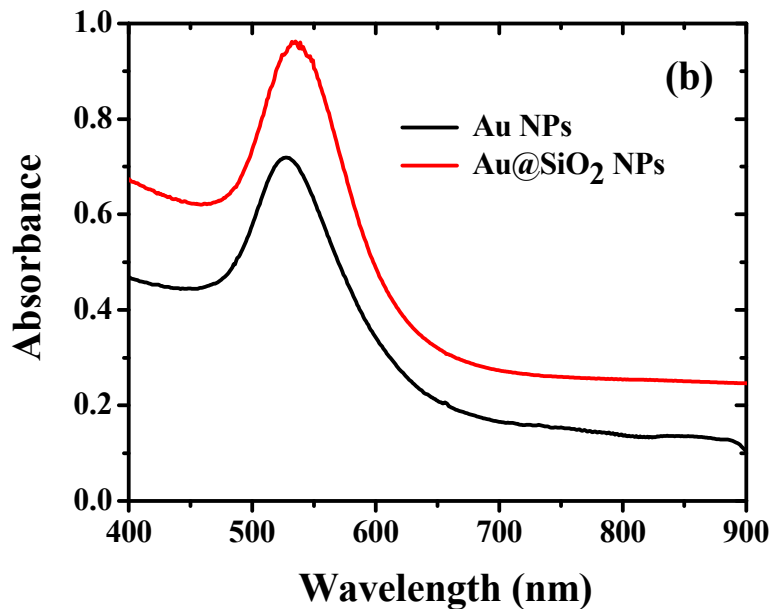


**Figure 2.** (a) TEM image of Au@SiO<sub>2</sub> core-shell NPs. (b) Absorption spectra of Au NPs with and without a SiO<sub>2</sub> shell in ethanol.

The SEM images of PEDOT: PSS films without and with Au@SiO<sub>2</sub> NPs are presented in Fig. 3a and 3b. Surface morphology of perovskite films coated on top of PEDOT: PSS without and with Au@SiO<sub>2</sub> NPs are shown by SEM and AFM images in Fig. 3c, 3d, 3e, and 3f, respectively. It was observed that the Au@SiO<sub>2</sub> NPs are distributed over the PEDOT: PSS layer as shown in Fig. 3b (tiny white spots on PEDOT: PSS film) and its corresponding perovskite film with Au@SiO<sub>2</sub> NPs exhibited a well uniform and compact film without any pinholes (Fig. 3d) compared to the perovskite film without Au@SiO<sub>2</sub> NPs (Fig. 3c). This is also supported in the AFM images (Fig. 3e and 3f). Thus, the perovskite film without Au@SiO<sub>2</sub> NPs showed a slightly non-uniform morphology with a roughness of 13.8 nm and have narrow gaps (see red circles in Fig. 3e) and small grain boundaries among perovskite crystals. In comparison, the perovskite films with Au@SiO<sub>2</sub> NPs show a decreased roughness (7.6 nm) and an absence of

narrow gaps among perovskite crystals. Such an improvement in the morphology of perovskite films is attributed to the interfacial modification of PEDOT: PSS film with Au@SiO<sub>2</sub> NPs. To further study the difference in morphology of perovskite films without and with Au@SiO<sub>2</sub> NPs, we performed XRD measurements on perovskite films deposited on PEDOT: PSS films without and with Au@SiO<sub>2</sub> NPs as shown in Fig. 4. In both cases, the perovskite films showed a similar diffraction pattern with nearly same intensity. This clearly indicates that Au@SiO<sub>2</sub> NPs are not influencing the crystallinity of perovskite films. A similar observation was also reported by Wu *et al.* in PSCs via the integration of Au@SiO<sub>2</sub> nanorods<sup>33</sup>. However, in this work, we have observed a slight difference in the morphology and uniformity in perovskite films after adding Au@SiO<sub>2</sub> NPs at an interface of PEDOT: PSS and perovskite layer.

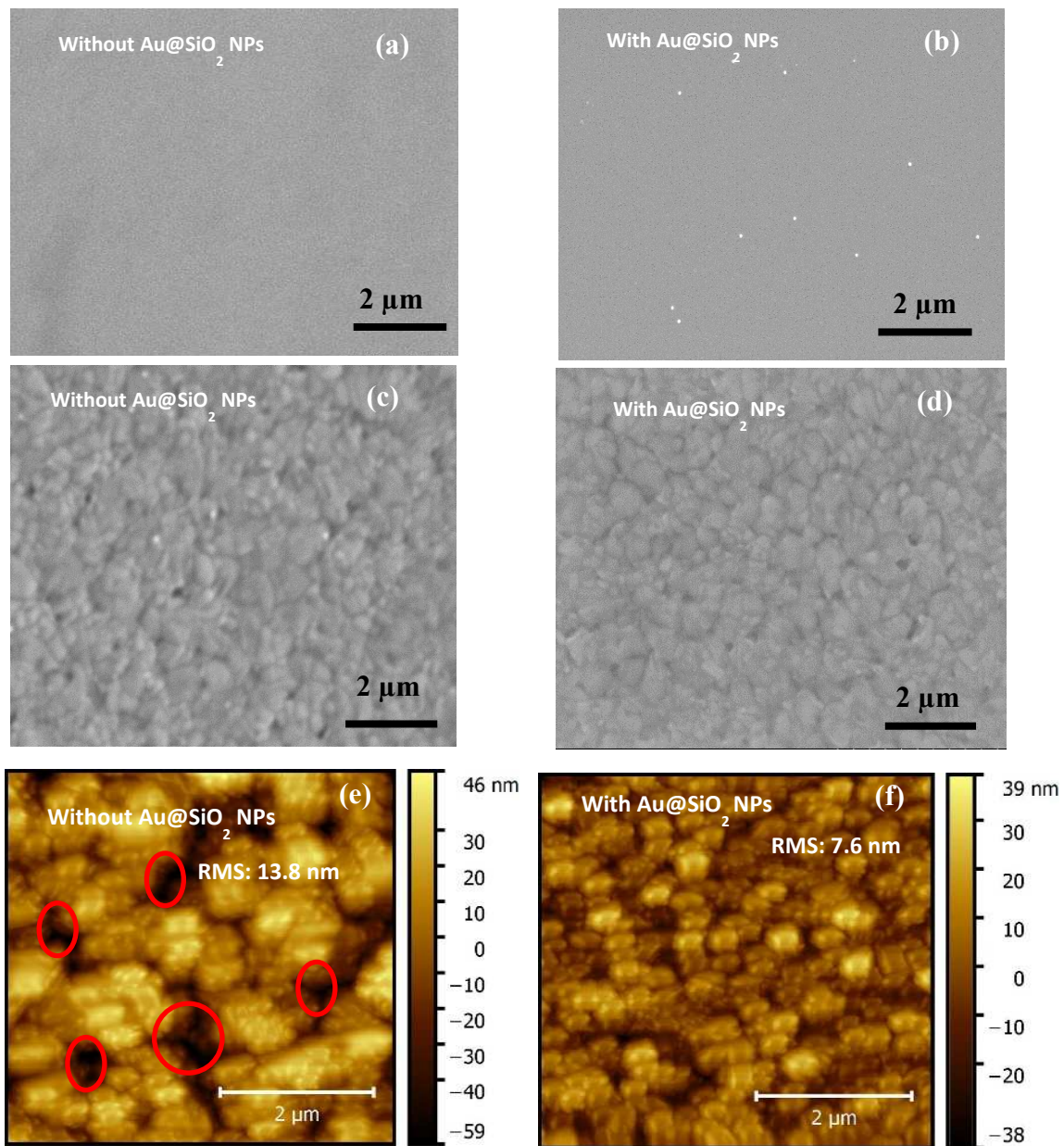


Figure 3. (a) and (b) SEM images of PEDOT:PSS films without and with Au@SiO<sub>2</sub> core-shell NPs, (c), (d), (e) and (f) SEM and AFM images of perovskite films without and with Au@SiO<sub>2</sub> core-shell NPs.

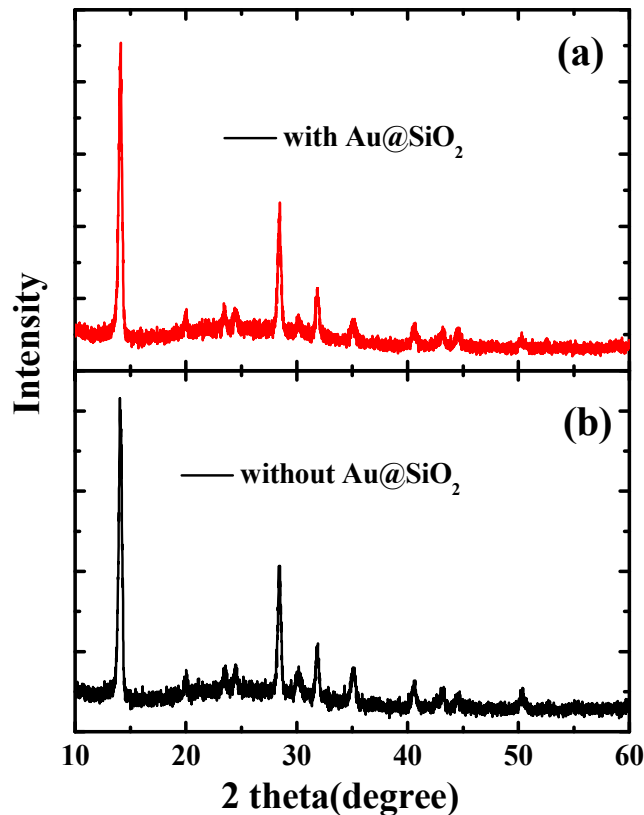


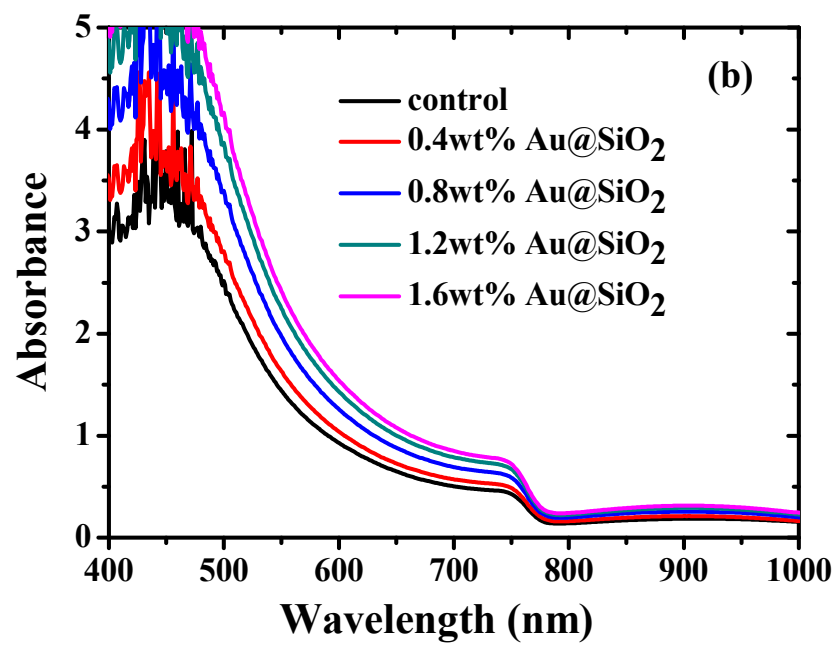
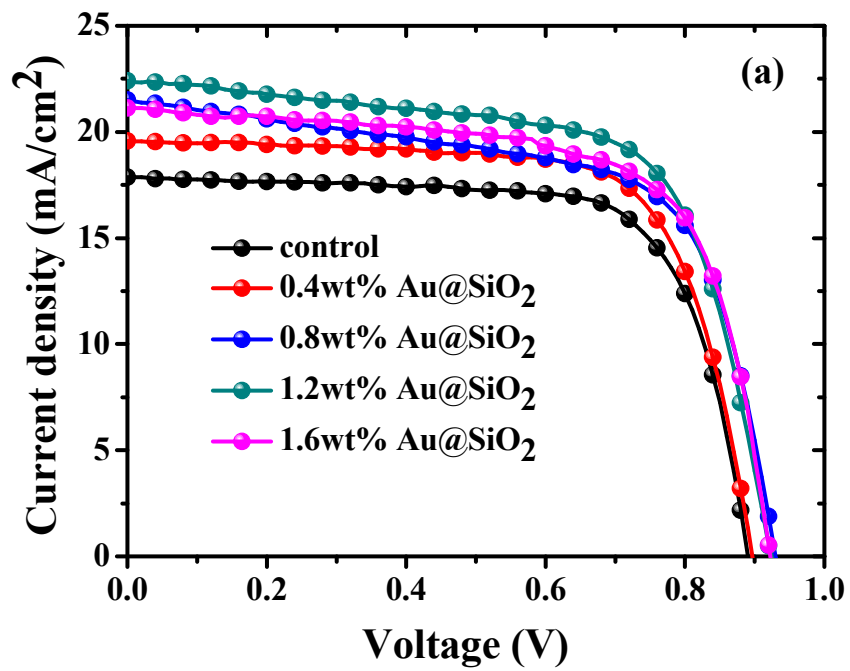
Figure 4. XRD patterns of Perovskite films (a) without and (b) with Au@SiO<sub>2</sub> core-shell NPs.

To investigate the role of Au@SiO<sub>2</sub> NPs on photovoltaic performance, PSCs without and with different concentrations of Au@SiO<sub>2</sub> NPs (0.4, 0.8, 1.2 and 1.6wt%) were fabricated. The J-V characteristics are presented in Fig. 5a and their photovoltaic parameters are summarized in Table 1. It was clearly observed that there is an enhancement in short-circuit density ( $J_{SC}$ ) and PCE, but a little change in open-circuit voltage ( $V_{OC}$ ) and fill factor (FF). The control devices without Au@SiO<sub>2</sub> NPs exhibited a  $J_{sc}$  of 17.45 mA/cm<sup>2</sup> and a PCE of 11.44 %. The PSC device with an optimized concentration (1.2wt%) of Au@SiO<sub>2</sub> NPs showed an improvement in  $J_{SC}$  by 25.1% from 17.45 to 22.35 mA/cm<sup>2</sup> and PCE by 27.3% from 11.44 to 14.57 %. This is a significant advancement over a recently reported  $J_{SC}$  (20.04 mA/cm<sup>2</sup>) and PCE (12.74%) by employing bare Au NPs in Spiro-OMeTAD hole transport layer solution<sup>27</sup>. The reliability data

also has included in Fig. 6 to ensure the improved photovoltaic performance of PSCs as a function of Au@SiO<sub>2</sub> NPs having different concentrations. In our case, the improvement in J<sub>SC</sub> and PCE is attributed to the insertion of Au@SiO<sub>2</sub> core-shell NPs between PEDOT: PSS film and perovskite film, which could efficiently trap the incident light and enhance the local electric field in the perovskite film. It is beneficial for improving the photovoltaic performance of PSCs by increasing light absorption in the device<sup>18, 34</sup>. Hsu *et al.* reported an improvement of J<sub>SC</sub> and PCE in organic solar cells and PSCs by integrating plasmonic Ag NPs with different sizes and shapes. The enhanced performance was attributed to the ability of plasmonic NPs to capture the light and increased the plasmonic scattering effect<sup>35</sup>. Qian *et al.* embedded plasmonic Ag NPs resonant at ~427 nm in PEDOT: PSS for mixed halide PSCs and reported that an enhancement in J<sub>SC</sub> and PCE are attributed to the improved hole extraction through the embedment of Ag NPs<sup>36</sup>. Snaith *et al.* also demonstrated the plasmonic improvement in the performance of PSCs by mixing Au@SiO<sub>2</sub> NPs into mesoporous Al<sub>2</sub>O<sub>3</sub>. The presence of SPR of Au NPs decreased the exciton binding energy within the perovskite material and resulted in a higher internal efficiency<sup>24</sup>. Recently, Long *et al.* reported the plasmonic improvement of PSC performance from a nanostructured Au electrode, which enhanced the light absorption and increased the optical path length of an active perovskite layer<sup>37</sup>. The above results and reports suggested that an improvement in photovoltaic performance of PSCs is attributed to the SPR increased optical absorption of plasmonic metal NPs.

To further confirm the improvement of J<sub>SC</sub> and PCE, UV-visible absorption and IPCE measurements were also carried out and their corresponding spectra are presented in Fig. 5b and 5c, respectively. Fig. 5b shows a linear enhancement in the absorption of perovskite films with the increasing concentration of Au@SiO<sub>2</sub> NPs. It was demonstrated that Au@SiO<sub>2</sub> NPs act as

subwavelength antennas to couple incident light into perovskite film, thereby improving the light absorption in perovskite film. An improved near field electric effect is also responsible for increasing optical absorption<sup>15</sup>. Therefore, resulted in an enhancement of PCE and  $J_{SC}$ . These results were consistent with the IPCE spectral response (Fig. 5c). Fig. 5c confirms that the photon to current conversion is improved with an increasing concentration of Au@SiO<sub>2</sub> NPs. The integrated  $J_{sc}$  is also calculated from the IPCE curves and is in good agreement with the  $J_{sc}$  values obtained from J-V curves. A significant enhancement in IPCE was obtained over the almost entire wavelength range (~350 to ~780 nm). In particular, the spectral response is highly improved in the range of ~400 to ~600 nm with increasing concentration of Au@SiO<sub>2</sub> NPs. This is attributed to the plasmonic effect of Au@SiO<sub>2</sub> NPs, which was caused by SPR absorption resonating at ~535 nm. In addition to the plasmonic effect, improved electrical properties could also contribute to an improvement in  $J_{sc}$ , PCE and spectral response<sup>33,38</sup>. Lee *et al.* reported that charge carrier recombination resistance increased by integrating plasmonic Au NPs in PSCs. This showed that the Au NPs not only improved the optical absorption but also enhanced the electrical properties of the device, therefore leading to a higher  $J_{SC}$  and PCE in devices<sup>27</sup>. In another study, it was found that the series resistance for PSCs with plasmonic metal NPs is lower than that of PSCs without plasmonic metal NPs. A higher shunt resistance and larger recombination resistance was also observed for PSCs with plasmonic metal NPs than those without metal NPs<sup>31</sup>. Thus, the improved electrical properties such as increased charge transport and decreased charge recombination could also be responsible for obtaining high  $J_{SC}$  and PCE apart from an enhanced optical absorption.



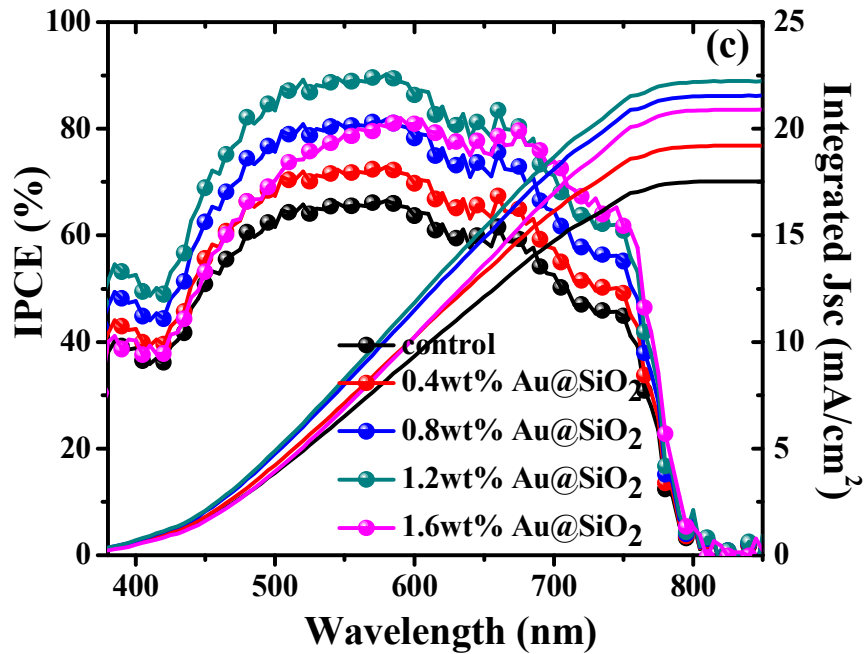


Figure 5. (a), (b) and (c): J-V characteristics, UV-visible absorption spectra and IPCE spectra of PSCs without and with Au@SiO<sub>2</sub> core-shell NPs at different concentrations.

Table 1. Photovoltaic parameters of PSCs without and with Au@SiO<sub>2</sub> core-shell NPs at different concentrations.

Device	V <sub>oc</sub> (V)	J <sub>sc</sub> (mA/cm <sup>2</sup> )	FF (%)	PCE (%)
Control	0.89 ± 0.02	17.45 ± 0.21	71.69 ± 0.25	11.44 ± 0.11
0.4wt% Au@SiO <sub>2</sub>	0.90 ± 0.01	19.57 ± 0.18	70.86 ± 0.19	12.48 ± 0.08
0.8wt% Au@SiO <sub>2</sub>	0.93 ± 0.01	21.56 ± 0.13	68.85 ± 0.21	13.80 ± 0.23
1.2wt% Au@SiO <sub>2</sub>	0.92 ± 0.02	22.35 ± 0.16	69.92 ± 0.28	14.57 ± 0.15
1.6wt% Au@SiO <sub>2</sub>	0.92 ± 0.02	21.13 ± 0.19	67.59 ± 0.24	13.14 ± 0.21

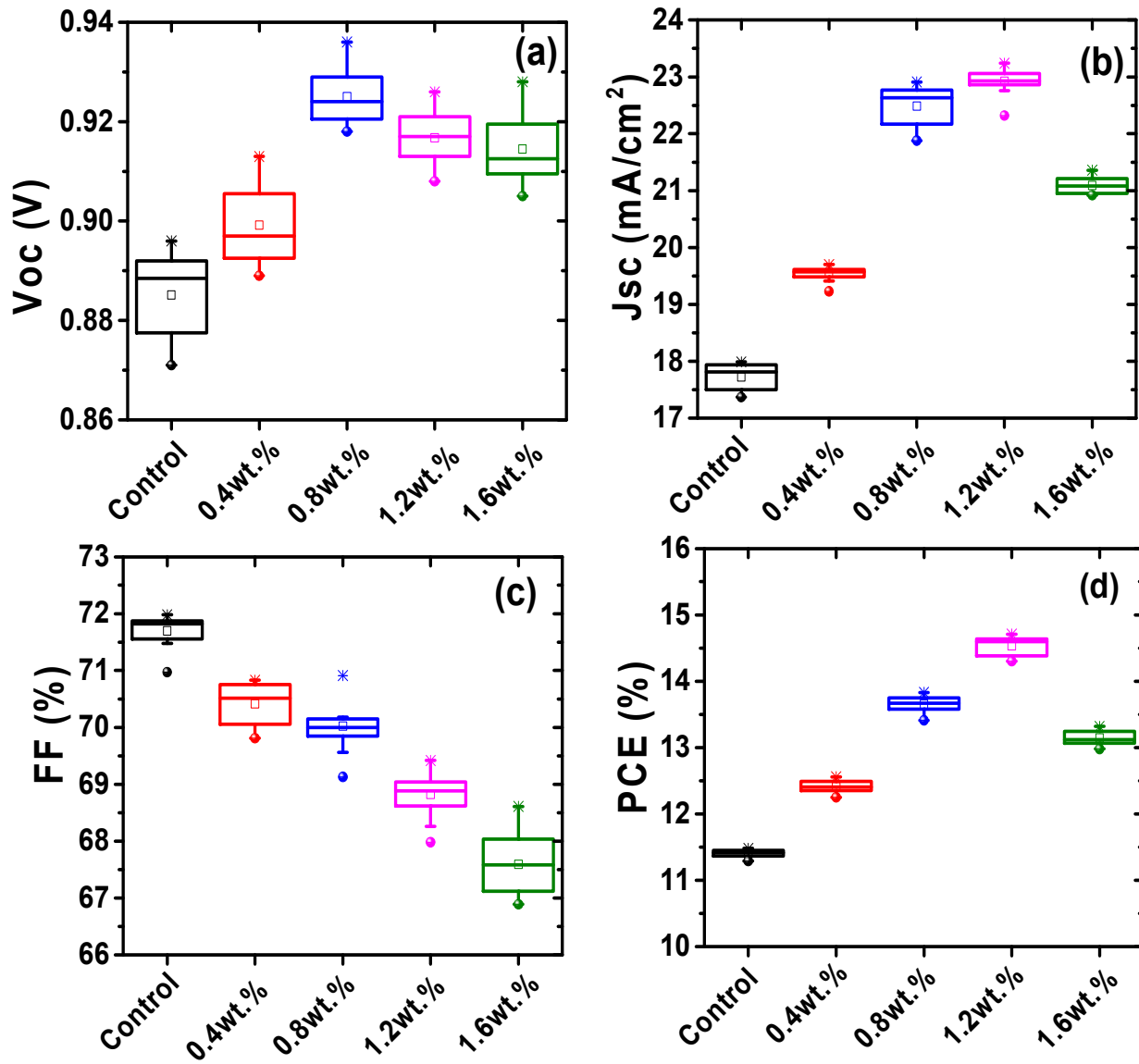


Figure 6. Photovoltaic parameters (a) Voc, (b) Jsc, (c) FF, and (d) PCE of PSCs as a function of different concentrations of Au@SiO<sub>2</sub> NPs.

**\*For each concentration twelve devices were fabricated.**

To understand the charge carrier dynamics, transient photocurrent (TPC) and transient photovoltage (TPV) decay measurements were recorded to find out charge transport time and charge carrier lifetime. Figs. 7a & b show mono-exponentially fitted decay and the corresponding raw data (insets) curves to calculate charge transport time and lifetime for the devices prepared with 1.2 wt.% and without Au@SiO<sub>2</sub> NPs. Table 2 shows charge transport time and lifetime values for devices prepared with and without Au@SiO<sub>2</sub>. To obtain an enhanced charge collection, a faster (shorter) charge transport time and slower (longer) charge lifetime values are desirable. It was observed that devices with Au@SiO<sub>2</sub> showed shorter charge transport time (0.665 μs) and longer lifetime (1.95 μs) as compared to devices made without Au@SiO<sub>2</sub> which showed charge transport time (0.782 μs) and lifetime (1.40 μs). A short charge transport time and long lifetime values will lead to an enhancement of charge collection in devices, resulting in higher device performance. The charge transport time and lifetime values obtained from TPC and TPV curves are in good agreement with a higher J<sub>sc</sub> and V<sub>oc</sub> in devices prepared with and without Au@SiO<sub>2</sub> NPs.

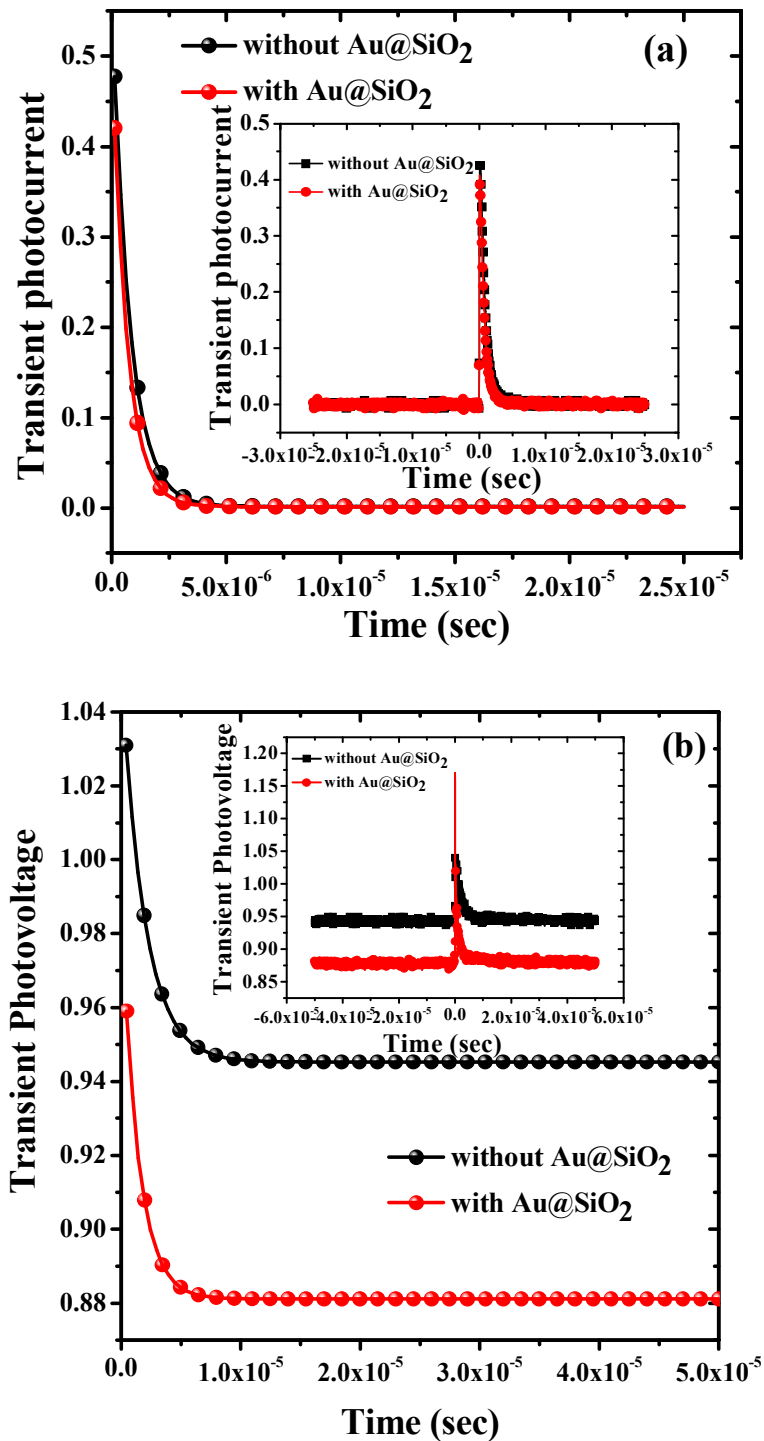


Figure 7. (a) Transient photocurrent decay and (b) transient photovoltage decay of PSCs prepared without and with Au@SiO<sub>2</sub>. The whole range of raw data is also shown in the insets of fig. a and b for corresponding transient photocurrent and photovoltage decay measurements.

Table 2. Charge transport time and lifetime for PSCs fabricated without and with Au@SiO<sub>2</sub>.

Device	Charge transport time	Charge carrier life time
Without Au@SiO <sub>2</sub>	$0.782 \times 10^{-6}$	$1.40 \times 10^{-6}$
With Au@SiO <sub>2</sub>	$0.665 \times 10^{-6}$	$1.95 \times 10^{-6}$

#### 4. Conclusions

In summary, we have demonstrated plasmonic effects of Au@SiO<sub>2</sub> core-shell NPs on the photovoltaic performance of planar heterojunction perovskite solar cells having an architecture of ITO/PEDOT: PSS/CH<sub>3</sub>NH<sub>3</sub>PbI<sub>3</sub>/PCBM/Rhodamine/Ag. Different concentrations of Au@SiO<sub>2</sub> NPs were introduced at the interface of PEDOT: PSS layer and perovskite layer. At an optimized concentration of Au@SiO<sub>2</sub> NPs, we achieved a significant improvement in J<sub>SC</sub> by 25.1% from 17.45 to 22.35 mA/cm<sup>2</sup> and PCE by 27.3% from 11.44 to 14.57%. The enhancement of device performance was attributed to an improved light trapping in the perovskite films by LSPR of Au@SiO<sub>2</sub> NPs and the spectral response was also improved, especially in the range of 400 to 600 nm, because of Au@SiO<sub>2</sub> NP's LSPR absorption resonating at around 535 nm. In addition, Au@SiO<sub>2</sub> NPs provided a shorter charge transport time and longer charge lifetime. This improved charge extraction and charge collection, resulting in an enhancement in J<sub>SC</sub> and PCE. Therefore, plasmonic metal NPs play a vital role in improving the photovoltaic performance of solar cells by enhancing light trapping and minimizing charge carrier recombination. The incorporation of plasmonic nanostructures has been demonstrated as one of the finest methods to enhance the J<sub>SC</sub> and PCE of solar cells.

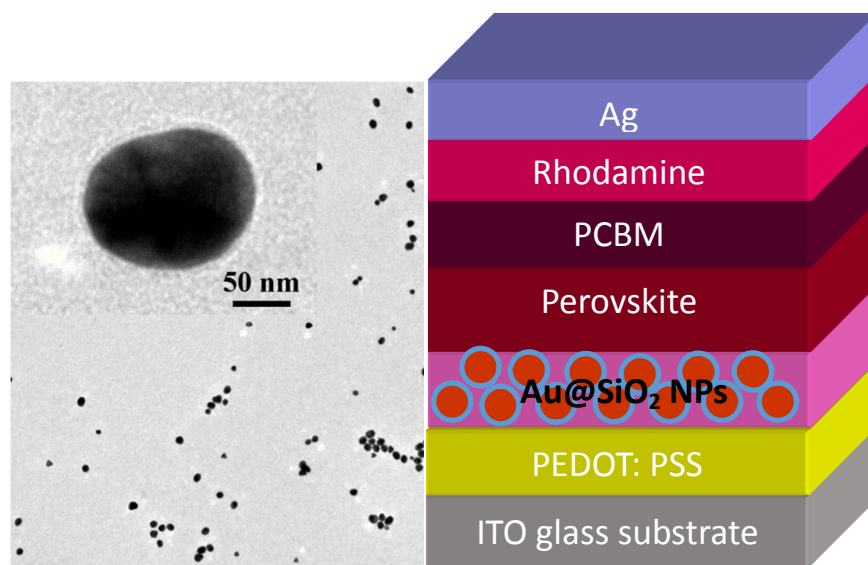
#### Acknowledgements

P. S. Chandrasekhar would like to thank Indo-US science and technology forum (IUSSTF) for providing an internship through Bhaskara Advanced Solar Energy Fellowship (BASE) program at South Dakota State University (SDSU), USA and thankful to Department of Science and Technology (DST), Govt. of India for offering fellowship under DST-INSPIRE fellowship program (IF-120755). This work was also partly supported by NSF MRI, NASA EPSCoR, US-Egypt Joint Science and Technology, and Pakistan-US Science and Technology Cooperation Program.

## References

1. L. Etgar, P. Gao, Z. Xue, Q. Peng, A. K. Chandiran, B. Liu, M. K. Nazeeruddin and M. Grätzel, *J. Am. Chem. Soc.*, 2012, **134**, 17396-17399.
2. J. Burschka, N. Pellet, S.-J. Moon, R. Humphry-Baker, P. Gao, M. K. Nazeeruddin and M. Grätzel, *Nature*, 2013, **499**, 316-319.
3. M. A. Green, K. Emery, Y. Hishikawa, W. Warta and E. D. Dunlop, *Prog. Photovolt: Res. Appl.*, 2015, **23**, 1-9.
4. H. J. Snaith, *J. Phys. Chem. Lett.*, 2013, **4**, 3623-3630.
5. H.-S. Kim, C.-R. Lee, J.-H. Im, K.-B. Lee, T. Moehl, A. Marchioro, S.-J. Moon, R. Humphry-Baker, J.-H. Yum, J. E. Moser, M. Grätzel and N.-G. Park, *Scientific Reports*, 2012, **2**, 591.
6. A. Kojima, K. Teshima, Y. Shirai and T. Miyasaka, *J. Am. Chem. Soc.*, 2009, **131**, 6050-6051.
7. H. Zhou, Q. Chen, G. Li, S. Luo, T.-b. Song, H.-S. Duan, Z. Hong, J. You, Y. Liu and Y. Yang, *Science*, 2014, **345**, 542-546.
8. W. S. Yang, J. H. Noh, N. J. Jeon, Y. C. Kim, S. Ryu, J. Seo and S. I. Seok, *Science*, 2015, **348**, 1234-1237.
9. <https://www.nrel.gov/pv/>.
10. M. Liu, M. B. Johnston and H. J. Snaith, *Nature*, 2013, **501**, 395-398.
11. A. Mei, X. Li, L. Liu, Z. Ku, T. Liu, Y. Rong, M. Xu, M. Hu, J. Chen, Y. Yang, M. Grätzel and H. Han, *Science*, 2014, **345**, 295-298.
12. P. You, Z. Liu, Q. Tai, S. Liu and F. Yan, *Adv. Mater.*, 2015, **27**, 3632-3638.
13. S. Das, B. Yang, G. Gu, P. C. Joshi, I. N. Ivanov, C. M. Rouleau, T. Aytug, D. B. Geohegan and K. Xiao, *ACS Photonics*, 2015, **2**, 680-686.

14. P. S. Chandrasekhar, N. Kumar, S. K. Swami, V. Dutta and V. K. Komarala, *Nanoscale*, 2016, **8**, 6792-6800.
15. H. A. Atwater and A. Polman, *Nat. Mater.*, 2010, **9**, 205-213.
16. H. Chen, L. Shao, Q. Li and J. Wang, *Chem. Soc. Rev.*, 2013, **42**, 2679-2724.
17. D. M. Schaadt, B. Feng and E. T. Yu, *Appl. Phys. Lett.*, 2005, **86**, 063106.
18. L. Lu, Z. Luo, T. Xu and L. Yu, *Nano Lett.*, 2013, **13**, 59-64.
19. S.-W. Baek, J. Noh, C.-H. Lee, B. Kim, M.-K. Seo and J.-Y. Lee, *Scientific Reports*, 2013, **3**, 1726.
20. K. Kim and D. L. Carroll, *Appl. Phys. Lett.*, 2005, **87**, 203113.
21. J. Qi, X. Dang, P. T. Hammond and A. M. Belcher, *ACS Nano*, 2011, **5**, 7108-7116.
22. P. Spinelli, V. E. Ferry, J. v. d. Groep, M. v. Lare, M. A. Verschuuren, R. E. I. Schropp, H. A. Atwater and A. Polman, *Journal of Optics*, 2012, **14**, 024002.
23. Y. H. Jang, Y. J. Jang, S. Kim, L. N. Quan, K. Chung and D. H. Kim, *Chem. Rev.*, 2016, **116**, 14982-15034.
24. W. Zhang, M. Saliba, S. D. Stranks, Y. Sun, X. Shi, U. Wiesner and H. J. Snaith, *Nano Lett.*, 2013, **13**, 4505-4510.
25. M. Saliba, W. Zhang, V. M. Burlakov, S. D. Stranks, Y. Sun, J. M. Ball, M. B. Johnston, A. Goriely, U. Wiesner and H. J. Snaith, *Adv. Funct. Mater.*, 2015, **25**, 5038-5046.
26. Z. Yuan, Z. Wu, S. Bai, Z. Xia, W. Xu, T. Song, H. Wu, L. Xu, J. Si, Y. Jin and B. Sun, *Adv. Energy Mater.*, 2015, **5**, 1500038-n/a.
27. D. S. Lee, W. Kim, B. G. Cha, J. Kwon, S. J. Kim, M. Kim, J. Kim, D. H. Wang and J. H. Park, *ACS Appl. Mater. Interfaces*, 2016, **8**, 449-454.
28. C. Graf, D. L. J. Vossen, A. Imhof and A. van Blaaderen, *Langmuir*, 2003, **19**, 6693-6700.
29. B. V. Enustun and J. Turkevich, *J. Am. Chem. Soc.*, 1963, **85**, 3317-3328.
30. J. Rodríguez-Fernández, I. Pastoriza-Santos, J. Pérez-Juste, F. J. García de Abajo and L. M. Liz-Marzán, *J. Phys. Chem. C*, 2007, **111**, 13361-13366.
31. M. D. Brown, T. Suteewong, R. S. S. Kumar, V. D'Innocenzo, A. Petrozza, M. M. Lee, U. Wiesner and H. J. Snaith, *Nano Lett.*, 2011, **11**, 438-445.
32. S. W. Sheehan, H. Noh, G. W. Brudvig, H. Cao and C. A. Schmuttenmaer, *J. Phys. Chem. C*, 2013, **117**, 927-934.
33. R. Wu, B. Yang, C. Zhang, Y. Huang, Y. Cui, P. Liu, C. Zhou, Y. Hao, Y. Gao and J. Yang, *J. Phys. Chem. C*, 2016, **120**, 6996-7004.
34. Z. Lu, X. Pan, Y. Ma, Y. Li, L. Zheng, D. Zhang, Q. Xu, Z. Chen, S. Wang, B. Qu, F. Liu, Y. Huang, L. Xiao and Q. Gong, *RSC Adv.*, 2015, **5**, 11175-11179.
35. H.-L. Hsu, T.-Y. Juang, C.-P. Chen, C.-M. Hsieh, C.-C. Yang, C.-L. Huang and R.-J. Jeng, *Sol. Energy Mater. Sol. Cells*, 2015, **140**, 224-231.
36. M. Qian, M. Li, X.-B. Shi, H. Ma, Z.-K. Wang and L.-S. Liao, *J. Mater. Chem. A*, 2015, **3**, 13533-13539.
37. M. Long, Z. Chen, T. Zhang, Y. Xiao, X. Zeng, J. Chen, K. Yan and J. Xu, *Nanoscale*, 2016, **8**, 6290-6299.
38. C. C. D. Wang, W. C. H. Choy, C. Duan, D. D. S. Fung, W. E. I. Sha, F.-X. Xie, F. Huang and Y. Cao, *J. Mater. Chem.*, 2012, **22**, 1206-1211.



We improved photovoltaic performance by about 29% in planar p-i-n perovskite solar cells (PSCs) using plasmonic Au@SiO<sub>2</sub> core-shell nanoparticles (NPs).